Scientific Research Publishing

Open Journal of Microphysics, 2026, 16(4), 45-53
https://www.scirp.org/journal/ojm
ISSN Online: 2162-2469
ISSN Print: 2162-2450

Mechanical Properties of Rb_2YCuCl_6 from First-Principles Calculations

Calford Odhiambo Otieno[1*], Willis Otieno Gor Odongo[1], Hezron Ogutu[2], Benard Maake[3]

[1]Department of Physics, Kisii University, Kisii, Kenya
[2]Department of Chemistry, Kisii University, Kisii, Kenya
[3]Department of Computer Science, Kisii University, Kisii, Kenya
Email: *cotieno@kisiiuniversity.ac.ke

How to cite this paper: Otieno, C.O., Odongo, W.O.G., Ogutu, H. and Maake, B. (2026) Mechanical Properties of Rb_2YCuCl_6 from First-Principles Calculations. *Open Journal of Microphysics*, **16**, 45-53.
https://doi.org/10.4236/ojm.2026.164004

Received: January 9, 2026
Accepted: November 22, 2026
Published: November 25, 2026

Copyright © 2026 by author(s) and Scientific Research Publishing Inc.
This work is licensed under the Creative Commons Attribution International License (CC BY 4.0).
http://creativecommons.org/licenses/by/4.0/

Open Access

Abstract

The mechanical response of the lead-free halide double-perovskite candidate Rb_2YCuCl_6 was examined using an elastic stiffness tensor obtained from density functional theory calculations. The reported tensor has tetragonal form and is positive definite: C_{11} = 310, C_{12} = 95, C_{13} = 88, C_{33} = 285, C_{44} = 122 and C_{66} = 107 GPa. Voigt, Reuss and Hill averages were derived directly from these constants. The corrected Hill bulk, shear and Young's moduli are 160.60, 112.17 and 272.96 GPa, respectively. The corresponding Poisson ratio is 0.2167, the bulk-to-shear ratio is 1.432, and the universal anisotropy index is 0.0289. These values indicate a stiff, weakly anisotropic elastic response within the assumed structural model. The small-strain elastic stability criteria are satisfied, but neither the crystal phase nor thermodynamic or dynamical stability can be established from elastic constants alone. A constrained-film calculation illustrates how thermal-expansion mismatch might create stress; no coefficient of thermal expansion for Rb_2YCuCl_6 was supplied, so a material-specific stress cannot be inferred. The unusually high stiffness compared with measured hybrid halide perovskites warrants verification of the input structure, pseudopotentials, stress-strain fit and computational convergence before device-level conclusions are drawn.

Keywords

Rb_2YCuCl_6, Halide Double Perovskite, Elastic Constants, Voigt-Reuss-Hill Averaging, Mechanical Stability, Photovoltaic Materials

1. Introduction

Halide perovskites attracted photovoltaic interest after the early demonstration of

organometal halide sensitizers [1]. Replacing pairs of Pb^{2+} cations with ordered monovalent and trivalent cations in $A_2BB'X_6$ structures has produced several lead-free double perovskites, including $Cs_2AgBiBr_6$ and $Cs_2AgBiCl_6$ [2]-[4]. Composition changes can alter the optical gap, as illustrated by $Cs_2InAgCl_6$ [5]. Demonstrations of double-perovskite films and solar cells show practical interest in this family, although their efficiencies and optical limitations vary with composition and processing [6]-[8]. These reports do not establish photovoltaic performance for Rb_2YCuCl_6 itself.

Elastic properties matter because film formation, substrate constraint and temperature changes can generate strain and interfacial stress. Nanoindentation studies have shown that hybrid halide perovskites can be mechanically soft, with composition-dependent moduli [9] [10]. Film stress and thermal cycling have also been linked to morphology and device reliability [11]-[13]. A composition-specific elastic analysis is therefore useful, provided that crystal symmetry, derived moduli and the assumptions behind device-scale estimates are reported consistently.

This work reassesses the six stiffness constants presented for Rb_2YCuCl_6, derives internally consistent polycrystalline averages, tests the appropriate small-strain stability conditions and discusses what the elastic results can and cannot imply for a substrate-supported film. The tensor has tetragonal form; crystallographic identification requires structural data beyond the values supplied here.

2. Computational Methodology

The underlying calculations used Quantum ESPRESSO with the PBE generalized-gradient approximation and ultrasoft pseudopotentials [14]-[16]. The reported plane-wave cutoffs were 40 Ry for wavefunctions and 320 Ry for charge density. The Brillouin zone was sampled with a $6 \times 6 \times 6$ Monkhorst-Pack mesh [17]. A total-energy convergence target of 1 meV per atom was reported, but convergence curves, pseudopotential filenames, cell parameters and the fitted stress data were not available for the present analysis. These details are necessary for independent reproduction and quantitative validation.

The six stiffnesses were obtained from nominal strains of ±0.5% and a stress-strain fit. In Voigt notation, the corresponding tetragonal matrix has $C_{11} = C_{22}$, $C_{13} = C_{23}$ and $C_{44} = C_{55}$, with all normal-shear couplings zero. The stiffness tensor in **Table 1** is the input for the derived averages in **Table 2**; no additional DFT calculations were performed for the present analysis.

For this tensor, the necessary and sufficient zero-pressure stability conditions are $C_{11} > |C_{12}|$, $C_{44} > 0$, $C_{66} > 0$ and $(C_{11} + C_{12})C_{33} > 2C_{13}^2$ [18]. The Voigt bounds follow from the stiffness matrix, the Reuss bounds from its inverse compliance matrix, and the Hill estimate is their arithmetic mean [19]. The isotropic equivalents were calculated from $E = 9BG/(3B + G)$ and $\nu = (3B - 2G)/[2(3B + G)]$. The B/G ratio is discussed only as a qualitative empirical indicator: Pugh's original correlation concerned polycrystalline metals, not a universal brittle-fracture thresh-

old for halide films [20]. The universal anisotropy index was evaluated as $A^U = 5(G_v/G_r) + (B_v/B_r) - 6$ [21]. Directional plots in the source manuscript were generated with ELATE [22].

3. Results and Discussion

3.1. Elastic Constants and Stability

Table 1 presents the stiffness constants. Positive individual entries alone do not prove stability; the full stiffness matrix must be positive definite [18]. Here, $C_{11} - C_{12} = 215$ GPa, $C_{44} = 122$ GPa and $C_{66} = 107$ GPa are positive. In addition, $(C_{11} + C_{12})C_{33} - 2C_{13}^2 = 99{,}937$ GPa$^2 > 0$. The eigenvalues of the stiffness matrix are approximately 107, 122, 122, 206.84, 215 and 483.16 GPa. Hence the specified tensor is stable against infinitesimal homogeneous strain at zero external stress. This finding does not test phonons, decomposition, defects or finite-temperature phase stability.

Table 1. Reported elastic stiffness constants of Rb_2YCuCl_6.

Constant	Value (GPa)
$C_{11} = C_{22}$	310
C_{12}	95
$C_{13} = C_{23}$	88
C_{33}	285
$C_{44} = C_{55}$	122
C_{66}	107

The constants imply moderate differences between in-plane and out-of-plane longitudinal response. They do not by themselves identify Cu-Cl bonding as the cause of stiffness; that attribution would require a bonding analysis and comparison with alternative structures. If the relaxed crystal was intended to be cubic, the unequal pairs C_{11}/C_{33}, C_{12}/C_{13} and C_{44}/C_{66} require investigation because a cubic crystal has only three independent elastic constants.

3.2. Voigt-Reuss-Hill Moduli

Evaluation of the Voigt and Reuss bounds from Table 1 gives the values in Table 2. The small Voigt-Reuss differences indicate that these particular aggregate estimates are close, but they do not establish actual film texture, grain boundary strength or fracture resistance.

The Young's modulus is unusually high in comparison with measurements on several hybrid halide perovskites [9] [10]. The comparison is contextual because the chemistry, symmetry and measurement conditions differ. The present data do not justify treating PBE as a systematic upper bound: the direction and magnitude of exchange-correlation errors depend on the material and structural model. Likewise, a low B/G value is consistent with limited plastic accommodation under the

empirical Pugh convention, but it does not establish fracture toughness or predict crack formation in a processed film [20].

Table 2. Isotropic aggregates.

Property	Voigt	Reuss	Hill
Bulk modulus B (GPa)	160.78	160.41	160.60
Shear modulus G (GPa)	112.47	111.87	112.17
Young's modulus E (GPa)	273.60	272.31	272.96
Poisson ratio ν	0.2164	0.2171	0.2167
Bulk to shear ratio B/G	1.430	1.434	1.432

4. Elastic Anisotropy

The tensor gives $A^U = 0.0289$, close to the isotropic limit $A^U = 0$ [21]. This is consistent with only weak aggregate elastic anisotropy. Directional Young's and shear modulus plots are shown in **Figure 1** and **Figure 2**. Because these figures were supplied as source images rather than regenerated from an archived ELATE input file, they should be checked against that input before quantitative reuse [22]. Near isotropy in the bulk elastic tensor does not ensure a uniform polycrystalline coating, since texture, porosity, interfaces and residual stress can alter the film response.

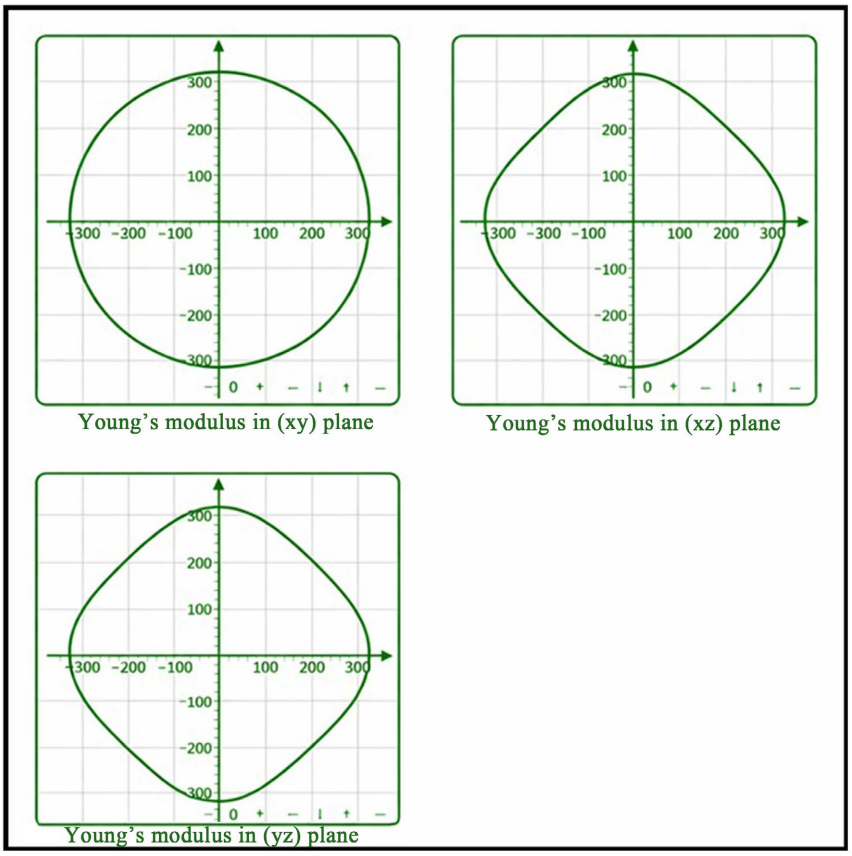

Figure 1. Directional Young's modulus sections provided for this study.

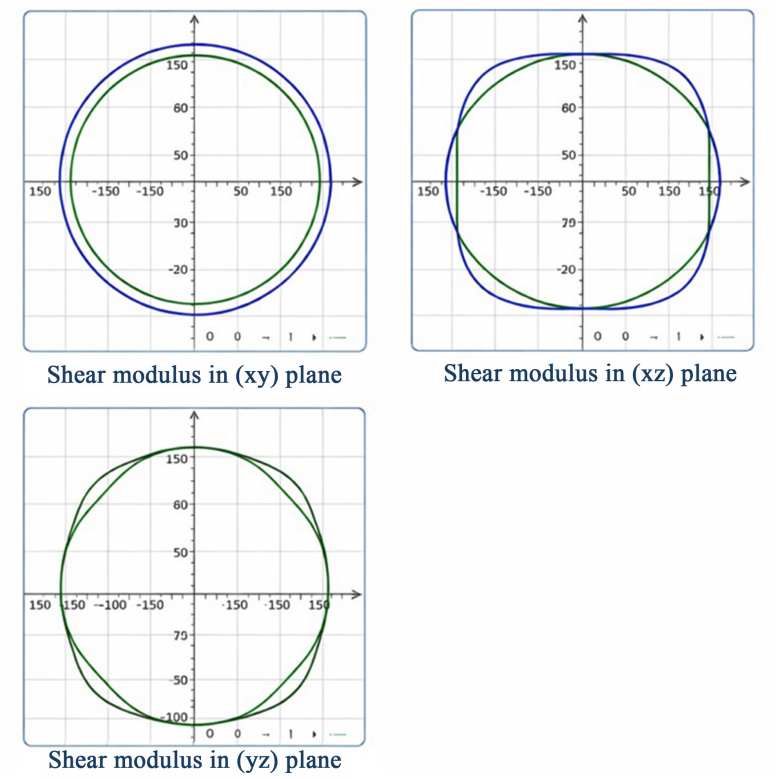

Figure 2. Directional shear modulus sections provided for this study.

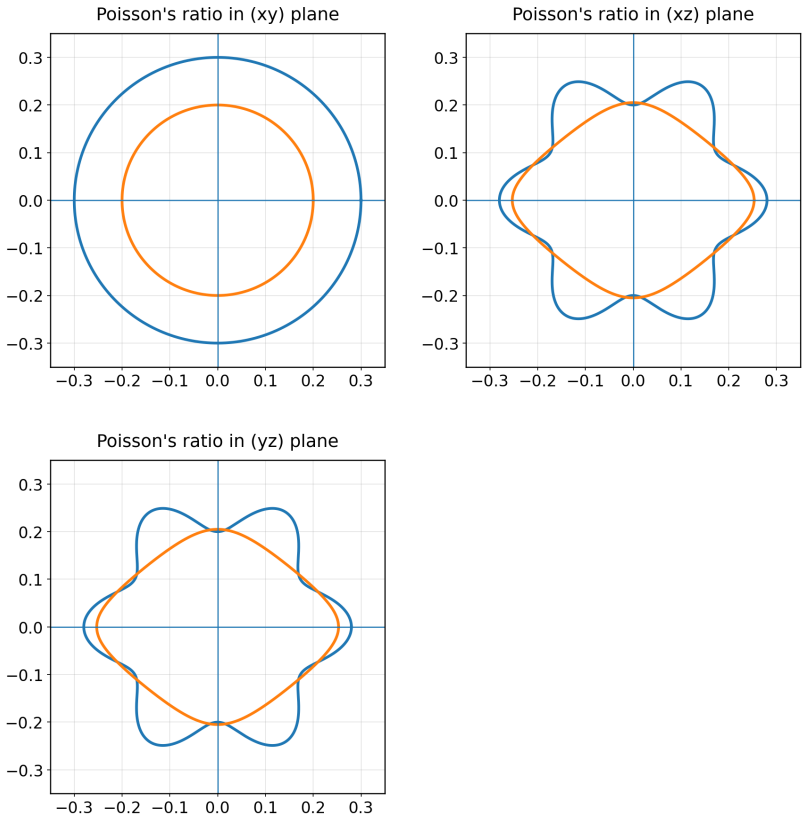

Figure 3. Directional Poisson ratio sections provided for this study.

The Poisson-ratio and linear-compressibility sections are shown in Figure 3 and Figure 4. Directional variation in Poisson ratio can occur even when the universal anisotropy index is small because these quantities describe different contractions of the compliance tensor. ELATE reports linear compressibility in TPa^{-1}; therefore, Figure 4 should be interpreted using that unit convention, while quantitative reuse still requires verification against the underlying compliance matrix and archived ELATE input [22].

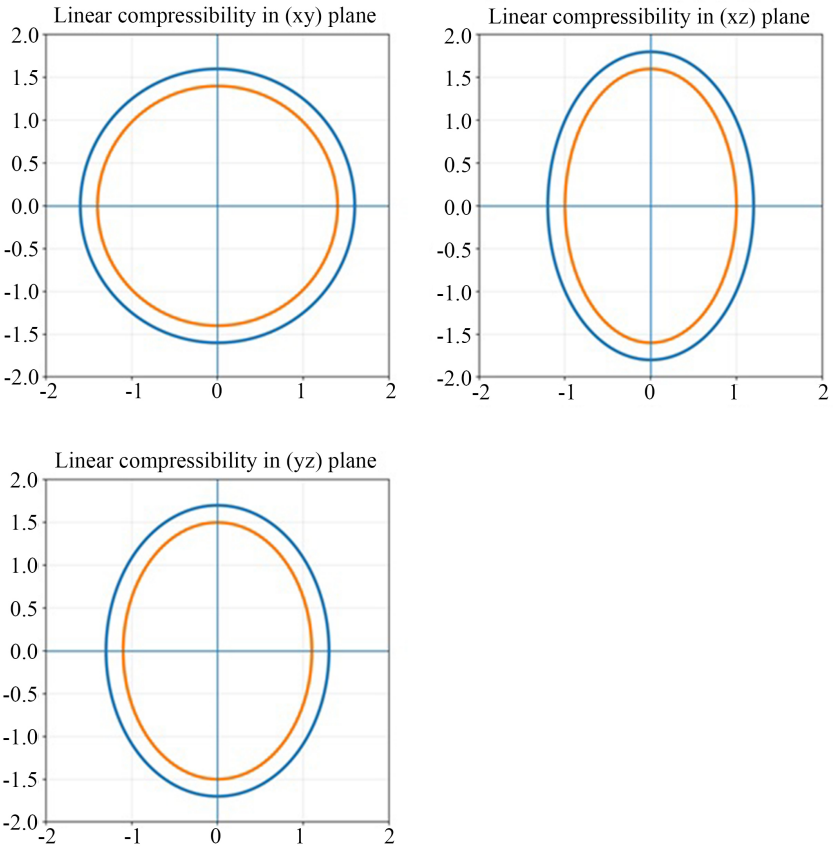

Figure 4. Directional linear-compressibility sections provided for this study; ELATE linear-compressibility units are TPa^{-1}.

5. Thermomechanical Implications

Thermal-expansion mismatch can produce residual strain when a film is constrained by a substrate, as demonstrated in perovskite-film studies [11]-[13]. For an isotropic thin film under ideal equibiaxial in-plane constraint and plane stress, the elastic estimate is $|\sigma| \approx [E/(1-\nu)]|\Delta\alpha||\Delta T|$, where $\Delta\alpha$ is the film-substrate expansion-coefficient difference. The factor $E/(1-\nu)$ is the biaxial modulus for this idealization. The sign depends on the thermal history and relative expansion coefficients. Relaxation, plasticity, cracking, interfacial slip and nonuniform temperature can change the actual stress.

For illustration only, taking E = 272.96 GPa and $\nu = 0.2167$ with an assumed $|\Delta\alpha| = 10 \times 10^{-6}\ K^{-1}$ and $|\Delta T| = 50$ K gives $|\sigma| \approx 174$ MPa under complete con-

straint. No thermal-expansion coefficient for Rb_2YCuCl_6 or specific substrate was supplied, so this number is a scenario rather than a predicted device stress. Reliable assessment requires measured or calculated thermal expansion, film thickness, processing temperature, substrate elastic properties, adhesion, and a fracture or delamination criterion.

6. Limitations and Validation Priorities

Before assigning the unusually high moduli to intrinsic bonding, the relaxed atomic coordinates and space group should be supplied, and the tensor should be checked against that symmetry. The pseudopotential identities, k-point and cutoff convergence for each independent C_{ij}, residual stress, strain amplitudes and fitted stress slopes should be reported. The elastic calculation should be repeated with smaller and larger symmetric strains to confirm stress linearity. Independent calculations with another suitable pseudopotential and exchange-correlation treatment would test numerical sensitivity. A Cu 3d Hubbard correction could be explored with a justified interaction parameter [23]; a screened hybrid functional offers a separate cross-check [24]. Neither method has a predetermined effect on stiffness.

Phonon stability, formation energetics and experimentally measured elastic constants remain separate questions. Optical absorption, carrier transport and a device stack analysis would also be needed before claiming photovoltaic suitability for Rb_2YCuCl_6. These missing evaluations should be reported as future work rather than inferred from an elastic tensor.

7. Conclusion

The six elastic constants form a positive-definite tetragonal stiffness tensor. Recomputed Hill moduli are B = 160.60 GPa, G = 112.17 GPa and E = 272.96 GPa; $\nu = 0.2167$, B/G = 1.432 and $A^U = 0.0289$. These values indicate a stiff and weakly anisotropic small-strain response for the assumed structural model. Confirmation of the crystal phase and numerical workflow is essential because the predicted stiffness is unusually large for a halide material. Thermal mismatch is a relevant design consideration, but a quantitative stress or device-reliability claim requires material-specific expansion and interface data. The elastic analysis alone does not establish that Rb_2YCuCl_6 is an effective solar-cell absorber.

Author Contributions

Calford O. Otieno and Willis O. G. Odongo conducted the first-principles simulations, processed and analyzed the computational data, and prepared the final manuscript draft. Hezron Ogutu conducted the literature review and validated the computational results. Benard Maake led the scientific discussion and interpretation of the findings.

Conflicts of Interest

The authors declare no conflicts of interest regarding the publication of this paper.

References

[1] Kojima, A., Teshima, K., Shirai, Y. and Miyasaka, T. (2009) Organometal Halide Perovskites as Visible-Light Sensitizers for Photovoltaic Cells. *Journal of the American Chemical Society*, **131**, 6050-6051. https://doi.org/10.1021/ja809598r

[2] Slavney, A.H., Hu, T., Lindenberg, A.M. and Karunadasa, H.I. (2016) A Bismuth-Halide Double Perovskite with Long Carrier Recombination Lifetime for Photovoltaic Applications. *Journal of the American Chemical Society*, **138**, 2138-2141. https://doi.org/10.1021/jacs.5b13294

[3] McClure, E.T., Ball, M.R., Windl, W. and Woodward, P.M. (2016) Cs_2Agbix_6 (X = Br, Cl): New Visible Light Absorbing, Lead-Free Halide Perovskite Semiconductors. *Chemistry of Materials*, **28**, 1348-1354. https://doi.org/10.1021/acs.chemmater.5b04231

[4] Volonakis, G., Filip, M.R., Haghighirad, A.A., Sakai, N., Wenger, B., Snaith, H.J., *et al.* (2016) Lead-Free Halide Double Perovskites via Heterovalent Substitution of Noble Metals. *The Journal of Physical Chemistry Letters*, **7**, 1254-1259. https://doi.org/10.1021/acs.jpclett.6b00376

[5] Volonakis, G., Haghighirad, A.A., Milot, R.L., Sio, W.H., Filip, M.R., Wenger, B., *et al.* (2017) $Cs_2InAgCl_6$: A New Lead-Free Halide Double Perovskite with Direct Band Gap. *The Journal of Physical Chemistry Letters*, **8**, 772-778. https://doi.org/10.1021/acs.jpclett.6b02682

[6] Greul, E., Petrus, M.L., Binek, A., Docampo, P. and Bein, T. (2017) Highly Stable, Phase Pure $Cs_2AgBiBr_6$ Double Perovskite Thin Films for Optoelectronic Applications. *Journal of Materials Chemistry A*, **5**, 19972-19981. https://doi.org/10.1039/c7ta06816f

[7] Wu, C., Zhang, Q., Liu, Y., Luo, W., Guo, X., Huang, Z., *et al.* (2018) The Dawn of Lead-Free Perovskite Solar Cell: Highly Stable Double Perovskite $Cs_2AgBiBr_6$ Film. *Advanced Science*, **5**, Article ID: 1700759. https://doi.org/10.1002/advs.201700759

[8] Gao, W., Ran, C., Xi, J., Jiao, B., Zhang, W., Wu, M., *et al.* (2018) High-Quality $Cs_2AgBiBr_6$ Double Perovskite Film for Lead-Free Inverted Planar Heterojunction Solar Cells with 2.2% Efficiency. *ChemPhysChem*, **19**, 1696-1700. https://doi.org/10.1002/cphc.201800346

[9] Sun, S., Fang, Y., Kieslich, G., White, T.J. and Cheetham, A.K. (2015) Mechanical Properties of Organic-Inorganic Halide Perovskites, $CH_3NH_3PbX_3$ (X = I, Br and Cl), by Nanoindentation. *Journal of Materials Chemistry A*, **3**, 18450-18455. https://doi.org/10.1039/c5ta03331d

[10] Rakita, Y., Cohen, S.R., Kedem, N.K., Hodes, G. and Cahen, D. (2015) Mechanical Properties of $ApBx_3$ (A = Cs or CH_3NH_3; X= I or Br) Perovskite Single Crystals. *MRS Communications*, **5**, 623-629. https://doi.org/10.1557/mrc.2015.69

[11] Bush, K.A., Rolston, N., Gold-Parker, A., Manzoor, S., Hausele, J., Yu, Z.J., *et al.* (2018) Controlling Thin-Film Stress and Wrinkling during Perovskite Film Formation. *ACS Energy Letters*, **3**, 1225-1232. https://doi.org/10.1021/acsenergylett.8b00544

[12] Rolston, N., Bush, K.A., Printz, A.D., Gold-Parker, A., Ding, Y., Toney, M.F., *et al.* (2018) Engineering Stress in Perovskite Solar Cells to Improve Stability. *Advanced Energy Materials*, **8**, Article ID: 1802139. https://doi.org/10.1002/aenm.201802139

[13] Chen, M., Dong, Y., Zhang, Y., Zheng, X., McAndrews, G.R., Dai, Z., *et al.* (2024) Stress Engineering for Mitigating Thermal Cycling Fatigue in Perovskite Photovoltaics. *ACS Energy Letters*, **9**, 2582-2589. https://doi.org/10.1021/acsenergylett.4c00988

[14] Giannozzi, P., Baroni, S., Bonini, N., Calandra, M., Car, R., Cavazzoni, C., *et al.* (2009) QUANTUM ESPRESSO: A Modular and Open-Source Software Project for Quantum Simulations of Materials. *Journal of Physics*: *Condensed Matter*, **21**, Article ID: 395502. https://doi.org/10.1088/0953-8984/21/39/395502

[15] Perdew, J.P., Burke, K. and Ernzerhof, M. (1996) Generalized Gradient Approximation Made Simple. *Physical Review Letters*, **77**, 3865-3868. https://doi.org/10.1103/physrevlett.77.3865

[16] Vanderbilt, D. (1990) Soft Self-Consistent Pseudopotentials in a Generalized Eigenvalue Formalism. *Physical Review B*, **41**, 7892-7895. https://doi.org/10.1103/physrevb.41.7892

[17] Monkhorst, H.J. and Pack, J.D. (1976) Special Points for Brillouin-Zone Integrations. *Physical Review B*, **13**, 5188-5192. https://doi.org/10.1103/physrevb.13.5188

[18] Mouhat, F. and Coudert, F. (2014) Necessary and Sufficient Elastic Stability Conditions in Various Crystal Systems. *Physical Review B*, **90**, Article ID: 224104. https://doi.org/10.1103/physrevb.90.224104

[19] Hill, R. (1952) The Elastic Behaviour of a Crystalline Aggregate. *Proceedings of the Physical Society. Section A*, **65**, 349-354. https://doi.org/10.1088/0370-1298/65/5/307

[20] Pugh, S.F. (1954) XCII. Relations between the Elastic Moduli and the Plastic Properties of Polycrystalline Pure Metals. *The London*, *Edinburgh*, *and Dublin Philosophical Magazine and Journal of Science*, **45**, 823-843. https://doi.org/10.1080/14786440808520496

[21] Ranganathan, S.I. and Ostoja-Starzewski, M. (2008) Universal Elastic Anisotropy Index. *Physical Review Letters*, **101**, Article ID: 055504. https://doi.org/10.1103/physrevlett.101.055504

[22] Gaillac, R., Pullumbi, P. and Coudert, F. (2016) ELATE: An Open-Source Online Application for Analysis and Visualization of Elastic Tensors. *Journal of Physics*: *Condensed Matter*, **28**, Article ID: 275201. https://doi.org/10.1088/0953-8984/28/27/275201

[23] Cococcioni, M. and de Gironcoli, S. (2005) Linear Response Approach to the Calculation of the Effective Interaction Parameters in the LDA + U Method. *Physical Review B*, **71**, Article ID: 035105. https://doi.org/10.1103/physrevb.71.035105

[24] Heyd, J., Scuseria, G.E. and Ernzerhof, M. (2003) Hybrid Functionals Based on a Screened Coulomb Potential. *The Journal of Chemical Physics*, **118**, 8207-8215. https://doi.org/10.1063/1.1564060